Alfvén Wave Excitation in a Cavity with a Transverse Magnetic Field

M. Bureš

Royal Institute of Technology, Department of Plasma Physics and Fusion Research, Stockholm, Sweden

Z. Naturforsch. **38 a**, 616–624 (1983); received January 24, 1983

A transversely magnetized cylindrical plasma model with an internal rod conductor is used to approximate the FIVA internal ring device of Spherator type with a purely poloidal magnetic field. It is shown that an excitation asymmetry along the plasma column, i.e. with a wave number $k_z \neq 0$, introduces a coupling between the magnetoacoustic and shear Alfvén waves in the frequency range $\omega \ll \omega_{ci}$. The introduction of an equilibrium mass motion along the plasma cylinder introduces a flow continuum. Simultaneously the Alfvén resonance frequency becomes Doppler shifted. The experimental observations indicate that cavity modes do not build up in the FIVA device in the case of nonsymmetric excitation. If on the other hand the exciting structure becomes symmetric, i.e. with $k_z = 0$, the magnetoacoustic resonances become excited. The resulting Q values are rather low which indicates that the coupling to the shear wave through the Hall electric field cannot be neglected.

1. Introduction

In most magnetic confinement systems there is a limit to the plasma temperature that can be reached by ohmic heating alone. To bring the plasma temperature to required values, a number of the additional heating methods are envisioned. Among these the low-frequency Alfvén wave heating has, for a number of years, attracted attention as a potentially powerfull means for heating a fusion plasma [1, 2]. If an oscillating magnetic field is applied externally to an inhomogeneous plasma, the wave energy is absorbed at the resonant surface where $\omega = k_\parallel V_A$, with $V_A = B_0(\mu_0 \varrho_0)^{-1/2}$ being the Alfvén speed and $k_\parallel$ the parallel wave number. In most of present day tokamaks the plasma density is too low for a simultaneous propagation of both the magnetoacoustic (M.A.) and shear Alfvén waves, i.e. only the shear wave is excited below the M.A. cut-off. With the increasing dimensions of future devices operating at higher densities, the energy coupling from an antenna to the Alfvén resonant layer via the M.A. wave becomes possible [3, 4, 5]. If the compressional plasma motion can be tolerated, this method offers a high antenna loading even for a relatively small coil. In the internal ring devices (INTRAP) the high density ($n \cong 10^{21}\ \mathrm{m}^{-3}$) plasmas are produced by means of an $\boldsymbol{E} \times \boldsymbol{B}$ discharge [6]. The M.A. modes were excited in the FIVA device [7] both at a low and a high power level. The frequency range of the operation above the M.A. cut-off allows for the excitation of shear Alfvén waves. The main feature of the INTRAP devices is the purely poloidal static magnetic field.

While tokamaks are approximated by an axially magnetized cylindrical plasma, we approximate the INTRAP device by a transversely magnetized plasma cavity with an internal cylindrical metallic wall [8]. The aim of this paper is to point out the specific features of the Alfvén wave excitation in this particular geometry.

Reprint requests to Prof. Dr. B. Lehnert, Dept. of Plasma Physics and Fusion Research, Royal Inst. of Technology, Teknikringen 33, S-10044 Stockholm, Sweden.

2. Basic equations

The small-amplitude waves in the frequency range well below the ion-cyclotron frequency are appropriately described by the linearized MHD equations. These can be written in the form

$$\mu_0 \varrho_0 \frac{\partial^2 \boldsymbol{\xi}}{\partial t^2} + \mu_0 \nabla p + \boldsymbol{B}_0 \times (\nabla \times \boldsymbol{B}) + \boldsymbol{B} \times (\nabla \times \boldsymbol{B}_0) = 0\,, \tag{1}$$

$$p + \gamma p_0 \nabla \cdot \boldsymbol{\xi} + \boldsymbol{\xi} \cdot \nabla p_0 = 0\,, \tag{2}$$

$$\boldsymbol{B} + \nabla \times (\boldsymbol{B}_0 \times \boldsymbol{\xi}) = 0\,, \tag{3}$$

where the quantities denoted by subscript 0 are the unperturbed equilibrium quantities, γ is the adia-

0340-4811 / 83 / 0600-0616 $ 01.3 0/0. – Please order a reprint rather than making your own copy.

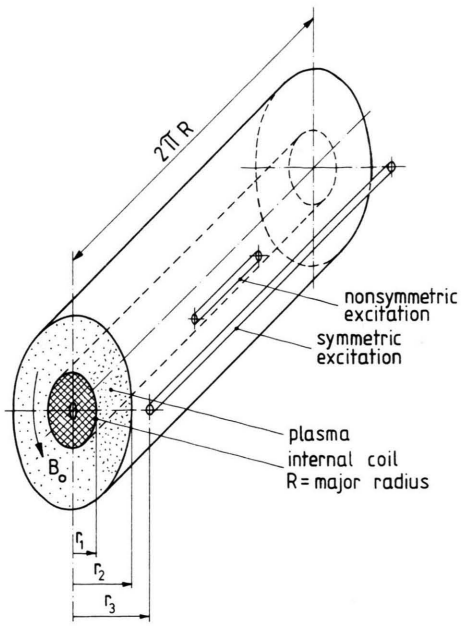

Fig. 1. The schematic diagram of the cavity geometry in the cylindrical approximation with the cases of symmetric and nonsymmetric excitation.

batic index and ξ, defined by $\boldsymbol{v} = \partial\xi/\partial t$, is the plasma displacement from an equilibrium position. Consider now a plasma cylinder with the static magnetic field $\boldsymbol{B}_0 = (0, B_0, 0)$ as shown in Fig. 1. The magnetic field is a function of the radius and satisfies the equilibrium condition

$$\frac{\mathrm{d}}{\mathrm{d}r}\left(p_0 + \frac{B_0^2}{2\mu_0}\right) + \frac{B_0^2}{\mu_0 r} = 0 . \tag{4}$$

We now assume an $f(r)\exp[i(m\varphi + k_z z - \omega t)]$ time and space dependence of the radio-frequency (RF) fields and introduce the total perturbed pressure $P = p + \boldsymbol{B}_0 \cdot \boldsymbol{B}/\mu_0$. The set of equations (1)–(4) can be reduced to a system of two first-order differential equations

$$D_1 \frac{\mathrm{d}}{\mathrm{d}r}(r\xi_r) = C_1 r \xi_r - r C_2 P , \tag{5}$$

$$D_1 \frac{\mathrm{d}}{\mathrm{d}r} P = \frac{1}{r} C_3 r \xi_r - C_1 P , \tag{6}$$

which, by eliminating of the variable P, results in a second order equation for the radial plasma displacement. It reads

$$\frac{\mathrm{d}}{\mathrm{d}r}\left[\frac{D_1}{C_2}\frac{1}{r}\frac{\mathrm{d}}{\mathrm{d}r}(r\xi_r)\right] + \frac{1}{D_1}\left(C_3 - \frac{C_1^2}{C_2}\right)\xi_r - r\xi_r \frac{\mathrm{d}}{\mathrm{d}r}\left(\frac{C_1}{r C_2}\right) = 0 . \tag{7}$$

Here

$$D_1 = \left[\gamma\beta\frac{V_A^2}{\omega^2}\left(\frac{\omega^2}{V_A^2} - \frac{m^2}{r^2}\right) + 1\right]\left(\frac{\omega^2}{V_A^2} - \frac{m^2}{r^2}\right),$$

$$C_1 = \frac{2}{r}\frac{V_A^2}{\omega^2}\left(\frac{\omega^2}{V_A^2} - \frac{m^2}{r^2}\right)\left(\frac{\omega^2}{V_A^2} - \gamma\beta\frac{m^2}{r^2}\right),$$

$$C_2 = \frac{1}{\omega^2 \varrho_0}\left\{\left(\frac{\omega^2}{V_A^2} - \frac{m^2}{r^2}\right)\left(\frac{\omega^2}{V_A^2} - \gamma\beta\frac{m^2}{r^2}\right) - k_z^2\left[\frac{\omega^2}{V_A^2} + \gamma\beta\left(\frac{\omega^2}{V_A^2} - \frac{m^2}{r^2}\right)\right]\right\},$$

$$C_3 = D_1\left[\frac{B_0^2}{\mu_0}\left(\frac{\omega^2}{V_A^2} - \frac{m^2}{r^2}\right) + \frac{2B_0}{\mu_0}\frac{\mathrm{d}}{\mathrm{d}r}\left(\frac{B_0}{r}\right)\right] + \mu_0\left(\frac{2B_0 V_A}{r\mu_0\omega}\right)^2\left(\frac{\omega^2}{V_A^2} - \frac{m^2}{r^2}\right)\left(\frac{\omega^2}{V_A^2} - \gamma\beta\frac{m^2}{r^2}\right),$$

where $V_A = B_0(\mu_0 \varrho_0)^{-1/2}$ is the Alfvén velocity and $\beta = \mu_0 p_0/B_0^2$. Eq. (7) is identical to that derived by Hain and Lüst [9] and Goedbloed and Hagebeuk [10]. However, the expressions for the coefficients D_1, C_1, C_2, C_3 are modified in accordance with the assumption of the steady magnetic field being purely poloidal. As pointed out by Appert et al. [11], (7) has two continuous spectra, i.e. the Alfvén continuum and slow wave continuum, i.e. a conclusion which can be drawn from (5) and (6) by putting $D_1 = 0$. Thus the shear Alfvén wave is described by

$$\frac{\omega^2}{V_A^2} = \frac{m^2}{r^2} , \tag{8}$$

and the continuum of slow wave is given by

$$\frac{\omega^2}{V_A^2}\left(\frac{1+\gamma\beta}{\gamma\beta}\right) = \frac{m^2}{r^2} . \tag{9}$$

It is interesting to observe that, even in the case of a homogeneous Alfvén speed, the shear wave has a continuous spectrum because of the radial dependence of the parallel wave number m/r. Equation (7) describes the magnetoacoustic and shear Alfvén

wave as well as the slow wave due to the finite pressure. The shear component B_z of the magnetic field reads

$$B_z = -k_z \frac{\mu_0 m}{r B_0}\left(\frac{\omega^2}{V_A^2} - \frac{m^2}{r^2}\right)^{-1} P . \tag{10}$$

2.1. Symmetric excitation

The toroidicity of the mode structure in the actual device is represented in the model by the axial wave number k_z. In a number of experiments with the FIV [12] and FIVA [13] device, the full-turn toroidal loops were used to excite the MHD modes. In the present model such a situation becomes equivalent to the consideration of modes with the wave number $k_z = 0$. Then the coefficients D_1, C_1 and C_2 of eqs. (5) and (6) become modified and read

$$D_1 = \gamma\beta \frac{V_A^2}{\omega^2}\left(\frac{\omega^2}{V_A^2} - \frac{m^2}{r^2}\right) + 1 ,$$

$$C_1 = \frac{2}{r}\frac{V_A^2}{\omega^2}\left(\frac{\omega^2}{V_A^2} - \gamma\beta\frac{m^2}{r^2}\right) ,$$

$$C_2 = \frac{1}{\omega^2 \varrho_0}\left(\frac{\omega^2}{V_A^2} - \gamma\beta\frac{m^2}{r^2}\right) ,$$

Thus eq. (7) is no more singular at the Alfvén layer, and consequently the shear wave is not excited by the excitation structure with $k_z = 0$. As can be seen from eq. (10), the shear and compressional waves are decoupled for $k_z = 0$. The slow wave is excited at the outermost plasma edges.

2.2. Cold plasma approximation

a) $\omega \ll \omega_{ci}$ range of frequencies

When the ion velocity of sound is small compared to the Alfvén velocity, the cold plasma approximation becomes adequate for describing the wave motion. The current needed to balance the zero order pressure gradient is neglected and (7) is reduced by putting $\beta = 0$. Further curl $\boldsymbol{B}_0 = 0$ is used to simplify the coefficient C_3. According to the simplified Ohm's law (eq. 3) the electric field component E_z is expressed as a function of plasma displacement.

$$E_z = i\omega B_0 \xi_r , \tag{11}$$

and we rewrite (7) in the form

$$\frac{d^2E_z}{dr^2} + \frac{1}{r}\left(1 - \frac{r k_z^2 D_1' \mu_0}{D_1 C_2 B_0^2}\right)\frac{dE_z}{dr} + \frac{B_0^2}{\mu_0} C_2 E_z = 0 . \tag{12}$$

Here

$$D_1 = \frac{\omega^2}{V_A^2} - \frac{m^2}{r^2} ,$$

$$C_2 = \frac{\mu_0}{B_0^2}\left(\frac{\omega^2}{V_A^2} - \frac{m^2}{r^2} - k_z^2\right) ,$$

and D_1' is the radial derivative of D_1. Close around the radius $r_c = m V_A/\omega$ eq. (12) has a solution [8]

$$E_z(r) = A I_0[k_z(r - r_c)] + B K_0[k_z(r - r_c)] . \tag{13}$$

$I_0[k_z(r - r_c)]$ and $K_0[k_z(r - r_c)]$ are the modified Bessel functions of zero order and A, B are amplitude constants. As $K_0(r)$ is not bounded at the origin, the amplitude of the E_z field diverges at r_c unless a damping is taken into consideration. The shear component B_z of the magnetic field diverges at the same layer;

$$B_z = \frac{k_z m \mu_0}{i\omega C_2 B_0^2}\frac{1}{r}\frac{dE_z}{dr} . \tag{14}$$

b) $\omega < \omega_{ci}$ range of frequencies

When the excitation frequency is not too low compared to ω_{ci}, the ion-cyclotron term $m_i \boldsymbol{j} \times \boldsymbol{B}_0/e\varrho_0$ has to be included in Ohm's law in order to describe the wave fields. Another situation, when this correction cannot be neglected, arises when the mode has a relatively high parallel wave number m/r or when the radius of the internal wall is small. In the case of excitation with $k_z = 0$, the electric wave field E_z is described by the following equation

$$\frac{d^2E_z}{dr^2} + \frac{1}{r}\frac{dE_z}{dr} + k_\perp^2(r) E_z = 0 , \tag{15}$$

where

$$k_\perp^2(r) = [(k_0^2 S - m^2/r^2)^2 - k_0^4 D^2]/(k_0^2 S - m^2/r^2) .$$

Here $S, \pm iD$ are dielectric tensor elements in Stix notation [14] which for frequencies $\omega \ll \omega_{ce}$, ω_{pe} reduce to $S = \omega_{pi}^2/(\omega_{ci}^2 - \omega^2)$ and $D = -\omega\omega_{pi}^2/[\omega_{ci}(\omega_{ci}^2 - \omega^2)]$. k_0 is a wave number in vacuum. The resonant layer position is now modified by the cyclotron correction

$$\frac{\omega^2}{V_A^2} = \left(1 - \frac{\omega^2}{\omega_{ci}^2}\right)\frac{m^2}{r^2} . \tag{16}$$

Eq. (15) has a regular solution of the type $(r - r_c)\log|(r - r_c)|$ at the Alfvén layer, but the shear component of the magnetic field is singular

there

$$B_z = \frac{m}{r\omega} \frac{i k_0^2 D}{\left(k_0^2 S - \frac{m^2}{r^2}\right)} E_z . \tag{17}$$

Disregarding the cylindrical nature of eq. (15) it is in principle the Budden type equation. Thus there is a fundamental difference in the solutions of eqs. (12) and (15). For arguments $k_z(r - r_c) \to 0$ the Bessel function $K_0[k_z(r - r_c)]$ is approximated by $-\log |k_z(r - r_c)|$. Just close to the critical layer, the B_z component given by eq. (14) diverges as $(r - r_c)^{-1}$ while eq. (17) diverges as $\log |(r - r_c)|$. $B_0^2 C_2 \mu_0^{-1}$ is approximated as $-k_z^2$ around the radius r_c, while $k_0^2 S - m^2/r^2$ is Taylor expanded there.

Consequently the shear magnetic field expressed by eq. (14) appears to be "more singular" than that given by eq. (17).

3. Alfvén waves in presence of an equilibrium mass flow

Consider a stationary mass flow $\boldsymbol{v}_0 = v_0 \hat{\mathbf{z}}$ created by the application of an electric field. In this model such a motion simulates that of a rotating plasma in toroidal geometry. Let us further assume that the plasma pressure is much lower than the magnetic field pressure ($\beta \ll 1$) and that the excitation frequency is well below the ion cyclotron frequency, i.e. $\omega \ll \omega_{ci}$. Then the general equations for the small-amplitude MHD waves in a medium in stationary equilibrium, given in the Appendix 1, reduce to

$$D_2 \frac{\mathrm{d}}{\mathrm{d}r}(r\,\xi_r) = C_4 r\,\xi_r - C_5 r P ,$$

$$D_2 \frac{\mathrm{d}}{\mathrm{d}r}(rP) = C_6 r\,\xi_r - D_2 P . \tag{18}$$

Here $P = B_0 B_\varphi / \mu_0$ and

$$D_2 = \left(1 - \frac{v_0}{v_{pz}}\right)\left[\frac{\omega^2}{V_A^2}\left(1 - \frac{v_0}{v_{pz}}\right)^2 - \frac{m^2}{r^2}\right],$$

$$C_4 = \left[\frac{\omega^2}{V_A^2}\left(1 - \frac{v_0}{v_{pz}}\right)^2 - \frac{m^2}{r^2}\right]\left[\frac{2}{r}\left(1 - \frac{v_0}{v_{pz}}\right) - \frac{1}{v_{pz}}\frac{\mathrm{d}v_0}{\mathrm{d}r}\right]$$

$$C_5 = \frac{\mu_0}{B_0^2}\left(1 - \frac{v_0}{v_{pz}}\right)^2\left[\frac{\omega^2}{V_A^2}\left(1 - \frac{v_0}{v_{pz}}\right)^2 - \frac{m^2}{r^2} - k_z^2\right],$$

$$C_6 = \frac{B_0^2}{\mu_0}\left[\frac{\omega^2}{V_A^2}\left(1 - \frac{v_0}{v_{pz}}\right)^2 - \frac{m^2}{r^2}\right]^2 ,$$

where $v_{pz} = \omega / k_z$ is the phase velocity in the z-direction. We conclude that eqs. (18) posses three singularities. The first appears when

$$v_{pz}\hat{\mathbf{z}} = \boldsymbol{v}_0 , \tag{19}$$

i.e., both the magnitude and the direction of the velocities are the same. The second and third singularities are described by

$$\frac{\omega^2}{V_A^2}\left(1 \mp \frac{v_0}{v_{pz}}\right)^2 - \frac{m^2}{r^2} = 0 . \tag{20}$$

For a fixed frequency and parallel wave number the Alfvén resonant layer is shifted towards higher densities for the wave propagating with a positive k_z [minus sign in eq. (20)]. In the case of a negative k_z the Alfvén layer is shifted towards the plasma edges. The density profile is assumed to be peaked at the plasma centre. The elimination of P from eqs. (18) results in a second order differential equation for ξ_r. In the case of the $k_z = 0$ symmetric excitation, eqs. (18) reduce to

$$\frac{\mathrm{d}^2 E_z}{\mathrm{d}r^2} + \frac{1}{r}\frac{\mathrm{d}E_z}{\mathrm{d}r} + \left(\frac{\omega^2}{V_A^2} - \frac{m^2}{r^2}\right) E_z = 0 . \tag{21}$$

We observe that the zero order flow velocity $\boldsymbol{v}_0$ does not modify the M.A. wave propagation. The M.A. wave is decoupled from the shear wave, which is not excited by the symmetric excitation even in the presence of the flow velocity $\boldsymbol{v}_0$. To illustrate the possible m-modes which can be excited in the cavity, the solutions of eqs. (8) and (20) are presented in Fig. 2 for the typical density and flow velocity profiles in the FIVA device. The case of nonsymmetric excitation is represented by the $k_z R = \pm 1{,}3$ modes, and symmetric excitation by $k_z R = 0$. The stability properties of the rotating plasma equilibria were treated in Refs. [15, 16].

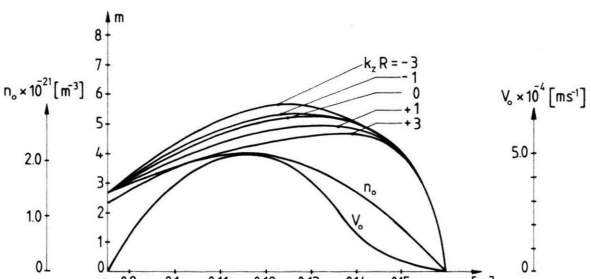

Fig. 2. The accessible parallel mode numbers for given equilibrium density and mass velocity profiles.

4. Boundary value solutions

To obtain the wave fields inside the plasma cavity, the appropriate boundary conditions have to be applied. Consider the cavity shown in Fig. 1 with the plasma surrounded by a vacuum and the excitation coil placed at the radius r_3. The tangential components of the electric and magnetic field are continuous across the plasma boundary at the radius r_2. The B_φ component has a discontinuity across the current layer $j^\#$ at the radius r_3. The condition which has to be fulfilled at the plasma boundary by the solution of eqs. (18) can be put in the form

$$E_z(r_2)\left[\frac{m^2}{r_2^2}\frac{K_m(k_z r_2)}{K'_m(k_z r_2)} - k_0^2\frac{K'_m(k_z r_2)}{K_m(k_z r_2)}\right] + i\omega k_z B_\varphi(r_2) + \frac{m^2}{r_2^2}\frac{v_0(r_2)}{v_{pz}}\left[1-\frac{v_0(r_2)}{v_{pz}}\right]^{-1}\frac{K_m(k_z r_2)}{K'_m(k_z r_2)}K_2^{-1}E_z(r_2) = i\omega\mu_0 j^\# k_z\frac{K_3}{K_2}. \quad (22)$$

Here

$$K_i = K_m(k_z r_i)/[I'_m(k_z r_i)K_m(k_z r_i) - I_m(k_z r_i)K'_m(k_z r_i)],$$

$i = 2, 3$ where I_m, K_m, I'_m, K'_m are the modified Bessel functions of the order m and their derivatives with respect to the argument $k_z r$. If the flow velocity v_0 is zero at the plasma boundary, the last term of the L.H.S. of eq. (22) disappears. We assume $k_0^2 \ll k_z^2$ for the vacuum field solutions. In the static case $v_0 = 0$, the B_φ component of the field can be expressed as

$$B_\varphi = \frac{i}{\omega}\left(\frac{\omega^2}{V_A^2} - \frac{m^2}{r^2}\right)\left(\frac{\omega^2}{V_A^2} - \frac{m^2}{r^2} - k_z^2\right)^{-1}\frac{dE_z}{dr}.$$

Finally, in the case of symmetric excitation ($k_z = 0$), eq. (22) reduces to

$$E_z(r_2) + \frac{r_2}{m}\frac{dE_z(r_2)}{dr} + i\omega r_2^m r_3^{-m+1}\mu_0 j^\#/m = 0.$$

Often, when solving for the wave equations, a damping is introduced to resolve the singularities.

A complex frequency $\omega + i\nu$ is then assumed. The reasonable estimate of the collision frequency ν in the frequency range $\omega \ll \omega_{ci}$ becomes (see Appendix 2)

$$\nu = \omega^2 \eta \varrho_0 B_0^{-2}.$$

Here $\eta = 129\,(\ln\Lambda)\,T^{-3/2}\,[\Omega\mathrm{m}]$ is the Spitzer resistivity.

5. Experimental arrangement

The experiments have been performed in the FIVA device which is schematically shown in Fig. 3. The topology of the confining magnetic field is purely poloidal. The average magnetic field strength in the equatorial plane is $B_0 \cong 0.35$ T. The hydrogen plasma is created by an $\boldsymbol{E}_0 \times \boldsymbol{B}_0$ discharge between the internal coil, which acts as anode, and two cathode rings. The plasma moves in the $\boldsymbol{E}_0 \times \boldsymbol{B}_0$ direction with a drift velocity $\boldsymbol{v}_0 = \boldsymbol{E}_0 \times \boldsymbol{B}_0/B_0^2$. The RF modes are excited both at low and high power levels. The latter is used to improve the signal to noise ratio when the radial wave field profiles are measured. The antenna current at a low power level is approximately $I_A = 5-10$ A while at the high level it becomes $I_A = 300-400$ A. A full turn antenna, exciting $k_z = 0$ symmetric modes, as well as a sector 90 degrees antenna were used. The RF magnetic field is measured by magnetic probes. The accuracy of the measurement is given by the reproducibility of the discharge. Fig. 4 shows the time evolution of the mean density while the figure inset shows a typical profile. Along the magnetic field, the plasma is confined to a region with an extension of about 0.2 m which is symmetric with respect to the equatorial plane. Thus the mode structure is mainly confined to this region. This implies a limit on the lowest parallel wave number accessible in the present discharges [7]. Typical plasma temperatures of the present discharges are $\langle T_0\rangle \cong 50000\,K$ which implies that the β values do not exceed $\cong 3{,}5\%$. The centrifugal force resulting from the equilibrium

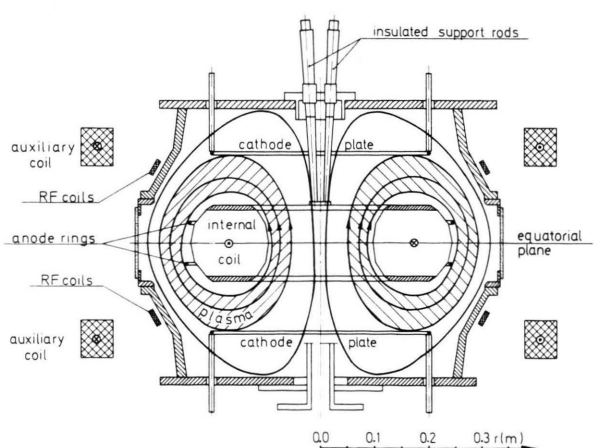

Fig. 3. The discharge chamber of the FIVA device. The shaded area indicates the plasma confinement region.

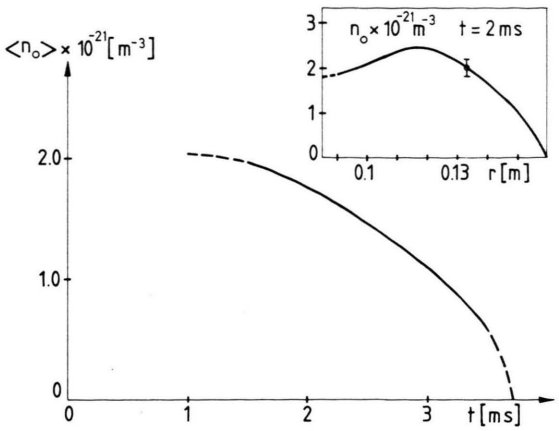

Fig. 4. The time evolution of the mean density $\langle n_0 \rangle$ during the discharge. The typical density profile $n_0(r)$ is plotted in the inset.

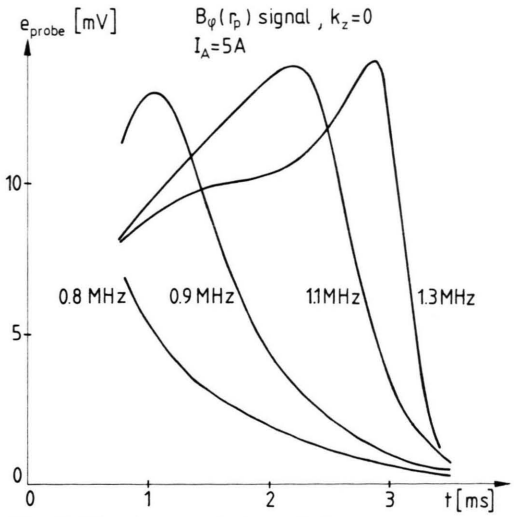

Fig. 5. The time evolution of the magnetoacoustic cavity signals excited by the symmetric, full-turn antenna. The radial position of the probe outside the plasma boundary is $r_p = 0.165$ m. The excitation frequency varies within the interval $\Delta f = 0.8 - 1.3$ MHz.

mass motion at the velocity v_0 is smaller than the ∇p_0 force. Thus the cold plasma approximation is adequate in describing the wave fields. The radial centrifugal force is not expected to introduce coupling between the M.A. and shear waves in the case of symmetric excitation.

6. Experimental results

6.1. Symmetric excitation

When the frequency is swept from below the cut-off for the M.A. waves, the B_φ signal measured outside the plasma boundary becomes as plotted in Fig. 5. The signal is normalized for an excitation current $I_A = 5$A. It was shown earlier [7] that, the lowest M.A. mode excited in the FIVA device becomes first radial ($r = 1$), $m = 3$ because of the parallel plasma confinement due to the centrifugal force. For the excitation frequency $f = 1.3$ MHz, the M.A. signal reveals the $r = 2$, $m = 3$ mode which is excited at $t \cong 1.6$ ms. It was further shown that the quality factor Q of these modes is low. This cannot be accounted for unless the confluence damping by the excitation of the shear wave is taken into account. In the low-frequency approximation the shear wave becomes uncoupled when excited by the full-turn antenna. Because the lowest parallel wave number accessible in the discharges is $m = 3$, the ion cyclotron correction becomes important enough to modify the M.A. mode propagation. The shear Alfvén wave is then no longer uncoupled and

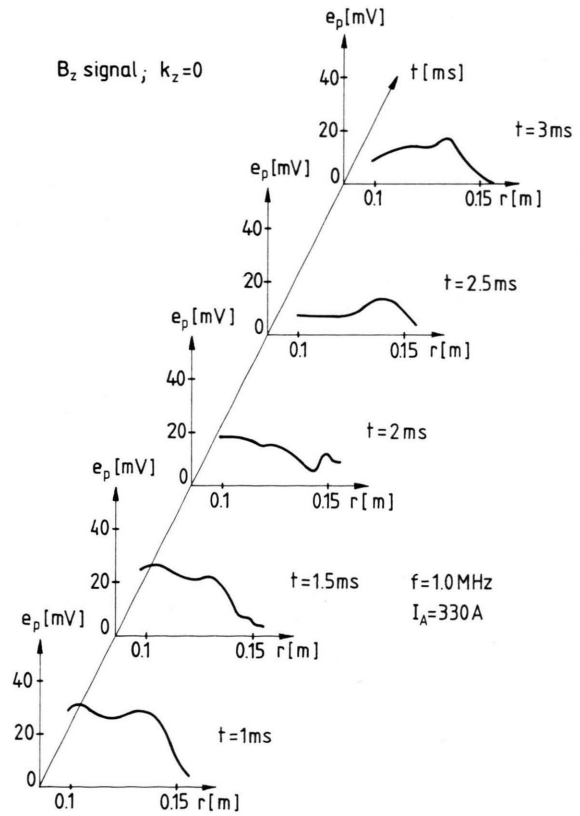

Fig. 6. The radial profiles of the shear Alfvén field excited at frequency $f = 1.0$ MHz by the symmetric, full-turn antenna.

becomes excited according to eq. (17). The radial profile evolution in time of the B_z shear component, excited at frequency $f = 1$ MHz, is plotted in Fig. 6. The profiles are rather broad, which indicates that even other than periodic modes along the field are excited. The amplitude of the B_z component is not correlated to the M.A. signal which has a typical time dependence as shown in Fig. 5. For the frequency 1 MHz, the M.A. signal has a resonance at the time $t \cong 2$ ms.

6.2. *Nonsymmetric excitation*

When the 90 degrees antenna is used, it is expected to excite $|k| = |k_z R| = 0, 1, 2, 3$ modes. Simultaneously the antenna coupling efficiency becomes roughly modified by the factor $\alpha \sin(k\alpha)/\pi k \alpha$, where $\alpha = \pi/4$ [17]. Consider a theoretical spectrum of the symmetric M.A. cavity modes accessible in the FIVA device together with the $r = 1$, $m = 3$, $k_z R = 1, 5$ cavity modes which are plotted in Fig. 7. If we assume that the damping is small, a rather high number of these modes will be excited within a small frequency interval when the density is kept constant. As an example, at the density $\langle n_0 \rangle = 10^{21}\ \mathrm{m}^{-3}$ all the $r = 1$, $m = 3$, $k_z R = \pm 0, 1, 2, 3, 4, 5$ modes will be excited within the frequency interval $\Delta f = 1.45 - 1.85$ MHz. However in the experiment, the $k_z \neq 0$ cavity modes are efficiently damped by the excitation of the localized shear Alfvén waves and only the symmetric $k_z = 0$ wave builds up a M.A. cavity mode. The time

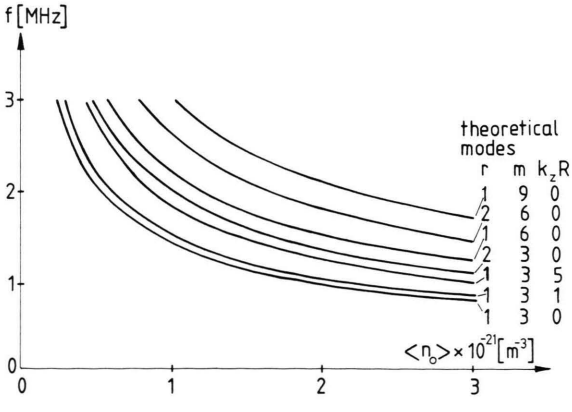

Fig. 7. The magnetoacoustic resonance spectrum of the plasma cavity shown in Figure 1. The adopted dimensions are: $r_1 = 0.085$ m, $r_2 = 0.16$ m and $R = 0.165$. The magnetic field strength is $B_0 = 0.35$ T.

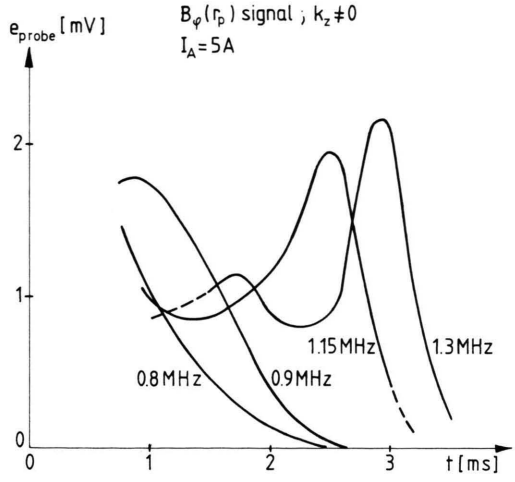

Fig. 8. The time evolution of the magnetoacoustic cavity signals excited by the nonsymmetric, 90° antenna. The radius of probe outside the plasma boundary is $r_p = 0.165$ m. The excitation frequency varies within the interval $\Delta f = 0.8 - 1.3$ MHz.

evolution of the B_φ signal (normalized to $I_A = 5$ A) excited at different frequencies and measured outside the plasma boundary is plotted in Fig. 8. It should be compared to signals shown in Fig. 5. We observe that the antenna coupling efficiency decreases approximately by the factor 7. This is a consequence of the antenna being only a 90 degree sector when compared to a full-turn loop. The coupling to the $r = 2$, $m = 3$ mode appears to be even smaller. If the decrease of coupling is taken into consideration and the signals are normalized for the same antenna current as in the symmetric case, the radial profiles of B_z field become as shown in Fig. 9. Some smaller peaks and oscillations presented there might be a result of the spread in data. Approximately 15 shots have to be taken to obtain the full profiles. Nevertheless the reproducibility of the results is good and the general character of the profiles, having the localized peaks, is clearly seen in contrast to the signals presented in Fig. 6. Despite the M.A. signal being close to the cut-off at the time $t = 2{,}5$ ms and below the cut-off at the time $t = 3$ ms, the shear Alfvén waves are excited with full amplitude. The high number of the Alfvén waves can be accounted for by the resonance splitting due to the zero order fluid motion v_0. Unfortunately, this feature cannot be studied in detail because the change of the fluid velocity v_0 results in a modification of the n_0 density profile. The amplitude of the

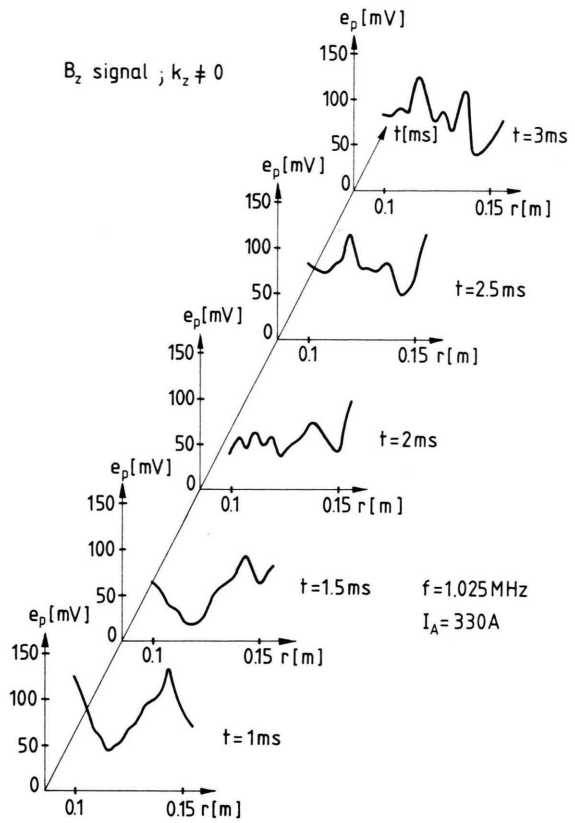

Fig. 9. The radial profiles of the shear Alfvén field excited at frequency $f = 1.025$ MHz by the nonsymmetric 90° antenna.

nonsymmetrically excited B_z field becomes enhanced by the factor 4 as compared to the symmetrically excited field.

This result demonstrates that the nonsymmetric excitation of the shear wave is more efficient than the excitation through the ion cyclotron term in the symmetric case. Because the antenna coupling efficiency decreases when departing from symmetry, the sector antenna need not be the optimal solution unless such a decrease is compensated by a higher antenna current. The sector antenna has a lower inductance because of its smaller geometrical dimensions. On the other hand, the antenna-plasma coupling can be improved by using several sectors. Nonsymmetric excitation is further preferable in the situations where the high fluid motion cannot be tolerated. Such a fluid motion would result from the excitation of the high Q M.A. modes.

7. Conclusions

The perturbations of a cylindrical equilibrium of a perfectly conducting plasma confined in purely poloidal static magnetic field contain the spectra of slow wave and shear Alfvén wave continua. In the case of symmetric excitation along the plasma column, the M.A. and shear wave are decoupled unless the magnetic field becomes sheared. The equilibrium pressure gradient ∇p_0 does not introduce any coupling. When an equilibrium mass motion is introduced along the axis of the plasma cylinder, an additional flow continuum is introduced.

The shear wave continuum is Doppler shifted up and down in frequency depending on the sign of $r_0 k_z/\omega$. In the case of the forced oscillations treated in this paper, the localized Alfvén resonance is split and shifted towards the plasma centre and plasma edge, respectively (for a density being peaked at the centre). The coupling between these modified resonances and the M.A. wave takes place only in the case of nonsymmetric ($k_z \neq 0$) excitation. For the flow continuum to come into operation, the velocity v_0 has to be high or the short wave-length modes in the v_0 direction have to be excited. The experimental observations in the FIVA device indicate that the coupling between the M.A. and shear waves through the ion-cyclotron term is less efficient in the case of the symmetric excitation than the coupling by asymmetric excitation. On the other hand the antenna coupling efficiency decreases rapidly with the reduction of the antenna length. That can be partly compensated by an increased antenna current because of the lower inductance, or by having a modified antenna arrangement consisting of several sectors. The $k_z \neq 0$ cavity modes were not excited in the experiment, thus demonstrating the efficiency of the localized damping by the shear Alfvén waves.

Acknowledgements

I thank Professor Bo Lehnert for his continuous interest in this work and Dr. A. Kuthy for the interesting discussions. I also thank Mr. J. Tonks for proof reading of the manuscript.

This work has been supported by the European Communities under an association contract between Euratom and Sweden.

Appendix 1

Perturbed stationary MHD equilibria

The linearized MHD equations for small-amplitude waves excited in a medium having an unperturbed stationary equilibrium can be written in the following form

$$\mu_0 \varrho_0 \left[\frac{d\boldsymbol{v}}{dt} + (\boldsymbol{v} \cdot \nabla)\, \boldsymbol{v}_0 \right] + \mu_0 \varrho (\boldsymbol{v}_0 \cdot \nabla)\, \boldsymbol{v}_0 \qquad \text{(A1)}$$

$$+ \mu_0 \nabla p + \boldsymbol{B}_0 \times (\nabla \times \boldsymbol{B}) + \boldsymbol{B} \times (\nabla \times \boldsymbol{B}_0) = 0\,,$$

$$\frac{d\varrho}{dt} + \nabla \cdot (\varrho_0 \boldsymbol{v}) = -\varrho \nabla \cdot \boldsymbol{v}_0, \qquad \text{(A2)}$$

$$\frac{dp}{dt} + \gamma p_0 \nabla \cdot \boldsymbol{v} + \boldsymbol{v} \cdot \nabla p_0 = -\frac{p}{p_0} \left(\frac{1-\gamma}{\gamma} \right) \boldsymbol{v}_0 \cdot \nabla p_0, \qquad \text{(A3)}$$

$$\frac{d\boldsymbol{B}}{dt} - \nabla \times (\boldsymbol{v} \times \boldsymbol{B}_0) - (\boldsymbol{B} \cdot \nabla)\, \boldsymbol{v}_0 = -\boldsymbol{B} \nabla \cdot \boldsymbol{v}_0, \qquad \text{(A4)}$$

where $\frac{d}{dt} = \frac{\partial}{\partial t} + \boldsymbol{v}_0 \cdot \nabla$ and $\boldsymbol{v}_0$ is the equilibrium mass velocity. When the plasma in the stationary equilibrium is incompressible, the R.H.S. of eqs. (A2)–(A4) become equal to zero.

Appendix 2

The estimation of the complex frequency $\omega + i\nu$

Let us introduce the collision momentum loss in the equation of motion in the form

$$-i\,\omega\,\varrho_0\,\boldsymbol{v} = \boldsymbol{j} \times \boldsymbol{B}_0 - \varrho_0\,\nu\,\boldsymbol{v}\,.$$

Then the combination with Ohm's law in the form

$$0 = \boldsymbol{E} + \boldsymbol{v} \times \boldsymbol{B}_0$$

results in

$$k_0^2\, S = \frac{\omega^2}{V_A^2} \left(1 + \frac{i\,\nu}{\omega} \right).$$

Here S is the perpendicular dielectric tensor element in Stix's notation. When the resistivity is introduced into the Ohm's law

$$\eta \boldsymbol{j} = \boldsymbol{E} + \boldsymbol{v} \times \boldsymbol{B}_0\,,$$

the combination with the equation of motion

$$-i\,\omega\,\varrho_0\,\boldsymbol{v} = \boldsymbol{j} \times \boldsymbol{B}_0$$

yields

$$k_0^2\, S \cong \frac{\omega^2}{V_A^2} \left(1 + \frac{i\,\omega\,\eta\,\varrho_0}{B_0^2} \right).$$

Consequently the equivalent collision frequency is expressed in the form

$$\nu = \omega^2\,\eta\,\varrho_0\,B_0^{-2}\,.$$

[1] A. Hasegawa and L. Chen, Phys. Rev. Letters. **32,** 454 (1974).
[2] J. A. Tataronis, J. Plasma Physics, **13,** part 1, 87 (1975).
[3] A. M. Messiaen, Proc. VIIth Europ. Conf. on Contr. Fusion and Plasma Phys., Lausanne 1975, Vol. I, 155.
[4] E. Ott et al., Phys. Fluids **21** (12), 2306 (1978).
[5] C. F. F. Kearney and F. W. Perkins, PPPL-1471, Plasma Phys. Laboratory, Princeton 1978.
[6] B. Lehnert, Nucl. Fusion **11,** 485 (1971).
[7] M. Bureš, Nucl. Instrum. Methods **206,** 517 (1983) and TRITA-PFU-80-08, RIT, Stockholm 1980.
[8] M. Bureš, Nucl. Instrum. Methods **205,** 219 (1983) and TRITA-PFU-79-06, RIT, Stockholm 1979.
[9] K. Hain and R. Lüst, Z. Naturforsch. **13 a,** 936 (1958).
[10] J. P. Goedbloed and H. J. L. Hagebeuk, Phys. Fluids **15,** 1090 (1972).
[11] K. Appert et al., Phys. Fluids **17** (7), 1471 (1974).
[12] B. Lehnert et al., Proc. IVth Int. Conf. on Plasma Phys. and Contr. Fusion Res., Madison IAEA-CN-28/A4, Vol. I, 59.
[13] M. Bureš, Phys. Scripta **27,** 83 (1983) and TRITA-PFU-82-02, RIT, Stockholm 1982.
[14] T. H. Stix, Theory of Plasma Waves. McGraw-Hill 1962.
[15] G. O. Spies, Phys. Fluids **21** (4), 580 (1978).
[16] T. A. K. Hellsten and G. O. Spies, Phys. Fluids **22** (4), 743 (1979).
[17] A. M. Messian et al., Nucl. Fusion **15,** 75 (1975).